Bayesian Network-based Mendelian Randomization for Variant Prioritization and Phenotypic Causal Inference

Jianle Sun, Jie Zhou, Yuqiao Gong, Chongchen Pang, Yanran Ma, Jian Zhao, Zhangsheng Yu, Yue Zhang

Supplementary Notes

SN1 Details about BNMR model

In the following we use notations in the calligraphic font $\mathcal{Z}$ to represent the set of variants, the bold font $\boldsymbol{Z}$ to represent the random vector of corresponding variants, and Italic capital letter Z to represent single variant.

As shown in Figure 1 & S1, in the learning stage, we introduce the DIE partitioning of the variant set $\mathcal{Z}$ according to the relationships with the exposure of interest X

$$\mathcal{Z} = \mathcal{Z}_D \cup \mathcal{Z}_I \cup \mathcal{Z}_E. \tag{S.1}$$

For each subject, the genotype of the whole genome is a random vector $\boldsymbol{Z} = (\boldsymbol{Z}_D^T, \boldsymbol{Z}_I^T, \boldsymbol{Z}_E^T)^T$ with each element equal to 0, 1, or 2, where $\boldsymbol{Z}_D$, $\boldsymbol{Z}_I$, and $\boldsymbol{Z}_E$ stand for the random vectors containing variants in subsets $\mathcal{Z}_D$, $\mathcal{Z}_I$, and $\mathcal{Z}_E$. variants in $\mathcal{Z}_D$ directly affect the exposure, variants in $\mathcal{Z}_I$ indirectly affect the exposure through gene interaction or linkage, and variants in $\mathcal{Z}_E$ do not affect the exposure. In other words, $\boldsymbol{Z}_E$ is independent with X ($X \perp\!\!\!\perp \boldsymbol{Z}_E$), $\boldsymbol{Z}_I$ is independent with X given $\boldsymbol{Z}_D$ ($X \perp\!\!\!\perp \boldsymbol{Z}_I | \boldsymbol{Z}_D$).

The three subsets can be distinguished via a directed acyclic graph (DAG) under the causal Markov, faithfulness, and sufficiency assumptions [1].

- Causal Markov assumption: Any node in a given network is conditionally independent of its non-descendents, given its parents. In other words, all variables that are d-separated in a DAG will be conditionally independent in the corresponding probability distribution.
- Causal Faithfulness assumption: No conditional independence relations other than the ones entailed by the Markov assumption are present in the population distribution. In other words, only the variables that are d-separated in a DAG will be independent.

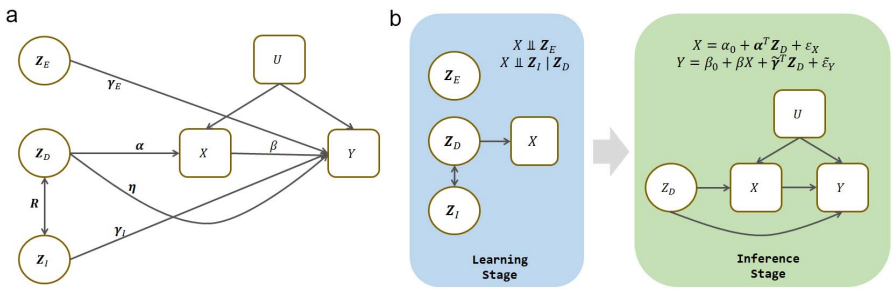

Figure S1: Notations in BNMR model.

- Causal Sufficiency assumptions: There are no unmeasured common causes of any pair of variables that are under consideration.

We transform the subset partition problem into a the structure learning of Bayesian networks (BN). A BN is a DAG $\mathcal{G} = \{\mathcal{V}, \mathcal{E}\}$ where nodes represent the variables while edges represent the conditional dependencies, with a collection of conditional probability distributions $\mathcal{O}$ that define the behavior of each variable given its parents. Scored-based approaches determine the optimal network by search all candidate graphs and maximizing the network score, such as the Bayesian information criterion (BIC) and the Bayes Dirichlet equivalent uniform (BDeu). These methods are computationally expensive, although greedy heuristics are often adopted to restricted the number of candidates. Meanwhile, constraint-based approaches employ a series of conditional independence tests to identify the edge constraints between nodes and then determine the directions by additional rules. It is usually faster, but often traps into the dilemma of Markov equivalent classes, on account of the same conditional independent patterns between the confounder and mediator [2]. Various algorithms can be implemented with R package bnlearn [3]

Since variants are causes of traits naturally according to the central dogma of molecular biology, the structure learning process can be further simplified to the determination of graph skeleton. Variants in $\mathcal{Z}_I$ and exposure X are D-separated by variants in $\mathcal{Z}_D$, and only the latter can be parents of X in the causal graph. Therefore, we identify variants in $\mathcal{Z}_D$ by scanning those nodes adjacent to X in the graph. The direction of edge variant-exposure is restricted as $Z_i \to X$ according to the central dogma of molecular biology. To simplify the computation, we introduce random graph forest (RGF), in which we sample n_s subjects and p_s features each time, and learn the network structure parallelly in all r subsamples. We then calculate the frequency of edge $Z_i - X$ in all subgraphs. The frequency is named as the adjacency score of Z_i, as an relative assessment of the relevance strength. Variants with the largest adjacency scores will be identified as Z_D and selected as IVs in the inference stage.

A quantitative trait is determined by both genotypic and environmental effects: $T = G + E$, where the mean environmental effect is usually taken to

be zero. Therefore, when the genotypes are fixed, the trait follows a Gaussian distribution $T|G \sim \mathcal{N}(G, \sigma_E^2)$. Therefore, X is determined by variants in $\mathcal{Z}_D$ and other environmental factors. Assuming linearity and no interaction, we have,

$$X = \alpha_0 + \boldsymbol{\alpha}^T \boldsymbol{Z}_D + \varepsilon_X, \tag{S.2}$$

where α represents the corresponding effect coefficients for X. Similarly, the outcome Y may be influenced by variants in $\mathcal{Z}_D$, $\mathcal{Z}_I$, and $\mathcal{Z}_E$,

$$Y = \gamma_0 + \boldsymbol{\gamma}_D^T \boldsymbol{Z}_D + \boldsymbol{\gamma}_I^T \boldsymbol{Z}_I + \boldsymbol{\gamma}_E^T \boldsymbol{Z}_E + \varepsilon_Y, \tag{S.3}$$

where β represents the corresponding effect coefficients for Y, and the error terms ε_X and ε_Y are correlated, but independent with $\boldsymbol{Z}$. Due to the horizontal pleiotropy, variants $Z_D \in \mathcal{Z}_D$ can affect Y through two different pathways: the vertical pleiotropy, which means Z_D affects Y through the exposure we studied (X), i.e., the causal pathway between X and Y ($Z_D \xrightarrow{\boldsymbol{\alpha}} X \xrightarrow{\beta} Y$); as well as the horizontal pleiotropy, which means Z_D affects the outcome directly or through other phenotypes ($Z_D \xrightarrow{\boldsymbol{\eta}} Y$). Under the assumption that horizontal pleiotropy effects are independent of the effects via the exposure (the InSIDE assumption) [4], we have,

$$\boldsymbol{\gamma}_D = \beta\boldsymbol{\alpha} + \boldsymbol{\eta}, \tag{S.4}$$

where β stands for the causal effect between exposure X and outcome Y, and $\boldsymbol{\eta}$ stands for the horizontal pleiotropy effects on Y of $\boldsymbol{Z}_D$.

For other variants, since $\boldsymbol{Z}_I$ is correlated to $\boldsymbol{Z}_D$ via gene interaction or linkage, we use $\boldsymbol{Z}_D$ to represent $\boldsymbol{Z}_I$ as

$$\boldsymbol{Z}_I = \boldsymbol{R}_0 + \boldsymbol{R}\boldsymbol{Z}_D + \boldsymbol{\varepsilon}_R, \tag{S.5}$$

where $\boldsymbol{R}$ represents the correlation matrix between $\boldsymbol{Z}_I$ and Z_D, $\boldsymbol{R}_0$ is independent with $\boldsymbol{Z}_D$, and $\boldsymbol{\varepsilon}_R$ is independent with $\boldsymbol{Z}_D$. On the other hand, $\boldsymbol{Z}_E$ is independent with $\boldsymbol{Z}_D$, then we can rewrite equation (6) as

$$\begin{aligned}
Y &= \gamma_0 + \boldsymbol{\gamma}_D^T \boldsymbol{Z}_D + \boldsymbol{\gamma}_I^T \boldsymbol{Z}_I + \boldsymbol{\gamma}_E^T \boldsymbol{Z}_E + \varepsilon_Y \\
&= \gamma_0 + (\beta\boldsymbol{\alpha} + \boldsymbol{\eta})^T \boldsymbol{Z}_D + \boldsymbol{\gamma}_I^T (\boldsymbol{R}_0 + \boldsymbol{R}^T \boldsymbol{Z}_D + \boldsymbol{\varepsilon}_R) + \boldsymbol{\gamma}_E^T \boldsymbol{Z}_E + \varepsilon_Y \\
&= \gamma_0 + \beta\boldsymbol{\alpha}^T \boldsymbol{Z}_D + (\boldsymbol{\eta} + \boldsymbol{R}\boldsymbol{\gamma}_I)^T \boldsymbol{Z}_D + (\boldsymbol{\gamma}_R^T \boldsymbol{R}_0 + \boldsymbol{\gamma}_E^T \boldsymbol{Z}_E) + \boldsymbol{\gamma}_I^T \boldsymbol{\varepsilon}_R + \varepsilon_Y \\
&= \beta X + (\boldsymbol{\eta} + \boldsymbol{R}\boldsymbol{\gamma}_I)^T \boldsymbol{Z}_D + (\gamma_0 + \boldsymbol{\gamma}_R^T \boldsymbol{R}_0 + \boldsymbol{\gamma}_E^T \boldsymbol{Z}_E - \beta\alpha_0) + (\boldsymbol{\gamma}_I^T \boldsymbol{\varepsilon}_R \\
&\quad + \varepsilon_Y - \beta\varepsilon_X) \\
&= \beta_0 + \beta X + \tilde{\boldsymbol{\gamma}}^T \boldsymbol{Z}_D + \tilde{\varepsilon}_Y,
\end{aligned} \tag{S.6}$$

where $\beta_0 = \gamma_0 + \boldsymbol{\gamma}_R^T \boldsymbol{R}_0 + \boldsymbol{\gamma}_E^T \boldsymbol{Z}_E - \beta\alpha_0$, $\tilde{\boldsymbol{\gamma}} = \boldsymbol{\eta} + \boldsymbol{R}\boldsymbol{\gamma}_I$, and $\tilde{\varepsilon}_Y = \boldsymbol{\gamma}_I^T \boldsymbol{\varepsilon}_R + \varepsilon_Y - \beta\varepsilon_X$. $\tilde{\varepsilon}_Y$ is independent with $\boldsymbol{Z}_D$. Then we have

$$\begin{aligned}
X &= \alpha_0 + \boldsymbol{\alpha}^T \boldsymbol{Z}_D + \varepsilon_X, \\
Y &= \beta_0 + \beta X + \tilde{\boldsymbol{\gamma}}^T \boldsymbol{Z}_D + \tilde{\varepsilon}_Y,
\end{aligned} \tag{S.7}$$

where ε_X and $\widetilde{\varepsilon}_Y$ are correlated, but both independent with $\boldsymbol{Z}_D$. The total error term ε_X and $\widetilde{\varepsilon}_Y$ can be decomposed into a confounding-related term and a completely random term, then we have $\mathbb{E}(\varepsilon_X) = \mathbb{E}(\widetilde{\varepsilon}_Y) = 0$, $\mathrm{Var}(\varepsilon_X) = \delta_1^2 + \sigma_1^2$, and $\mathrm{Var}(\widetilde{\varepsilon}_Y) = \delta_2^2 + \sigma_2^2$.

It is not necessary to identify all variants in $\mathcal{Z}_D$. We only need to select a subset of $\mathcal{Z}_D$ as instruments. In other words, it is essential to identify $\mathcal{Z}_D$ via BN learning with a high specificity instead of sensitivity. If we select genetic $Z_j \in \mathcal{Z}_D$ $(j = 1, 2, \ldots, J)$ as instruments, we have the Bayesian MR model [5]

$$\begin{aligned} X \mid Z, U &\sim \mathcal{N}(\alpha_0 + \sum_{j=1}^{J} \alpha_j Z_j + \delta_1 U, \sigma_1^2) \\ Y \mid X, Z, U &\sim \mathcal{N}(\beta_0 + \beta X + \sum_{j=1}^{J} \gamma_j Z_j + \delta_2 U, \sigma_2^2), \\ U &\sim \mathcal{N}(0, 1). \end{aligned} \tag{S.8}$$

The explicit modeling of pleiotropic effects brings nuisance parameters. To make the causal effect of interest β identifiable, we make an assumption that not all instruments included in the model have non-zero pleiotropic effect. And therefore, we impose a shrinkage prior on $\boldsymbol{\gamma}$ under the Bayesian framework [5]. Each component of $\boldsymbol{\alpha}$ has an independent Gaussian prior, and uninformative uniform priors are used for the other parameters.

Therefore, the BNMR model can be used to estimate the causal effect between exposure and outcome in two steps. In the learning stage, $\mathcal{Z}_D$ is distinguished from $\mathcal{Z}_I$ and $\mathcal{Z}_E$ through BN structure learning with all the variants and exposure X. In the inference stage, using selected Z_j as IVs, the causal effects can be estimated via the above Bayesian MR equation (S.8).

For non-Gaussian distributed outcomes, we introduce the link function $h(\cdot)$ for transformation, i.e.

$$h(\mathbb{E}(Y \mid X, Z, U)) = \beta_0 + \beta X + \sum_{j=1}^{J} \gamma_j Z_j + \delta_2 U. \tag{S.9}$$

For example, we can use logistic regression for binary outcome, and here the link function $h(y) = \mathrm{logit}(y) = \log \frac{y}{1-y}$.

SN2 Adjacency score and relevance strength

When all variants are included in each subsample ($p_s = p$), the adjacency score of a particular variant Z_i can be regarded as the confidence of the edge $Z_i - X$ in the average graph, or the probability that Z_i belongs to subset $\mathcal{Z}_D$. When $p_s < p$, the adjacency score can be regarded as the "relative probability" that Z_i belongs to subset $\mathcal{Z}_D$ since all variants share the same likelihood to be sampled in each subgraph. Variants with higher adjacency score are more reliable to affect

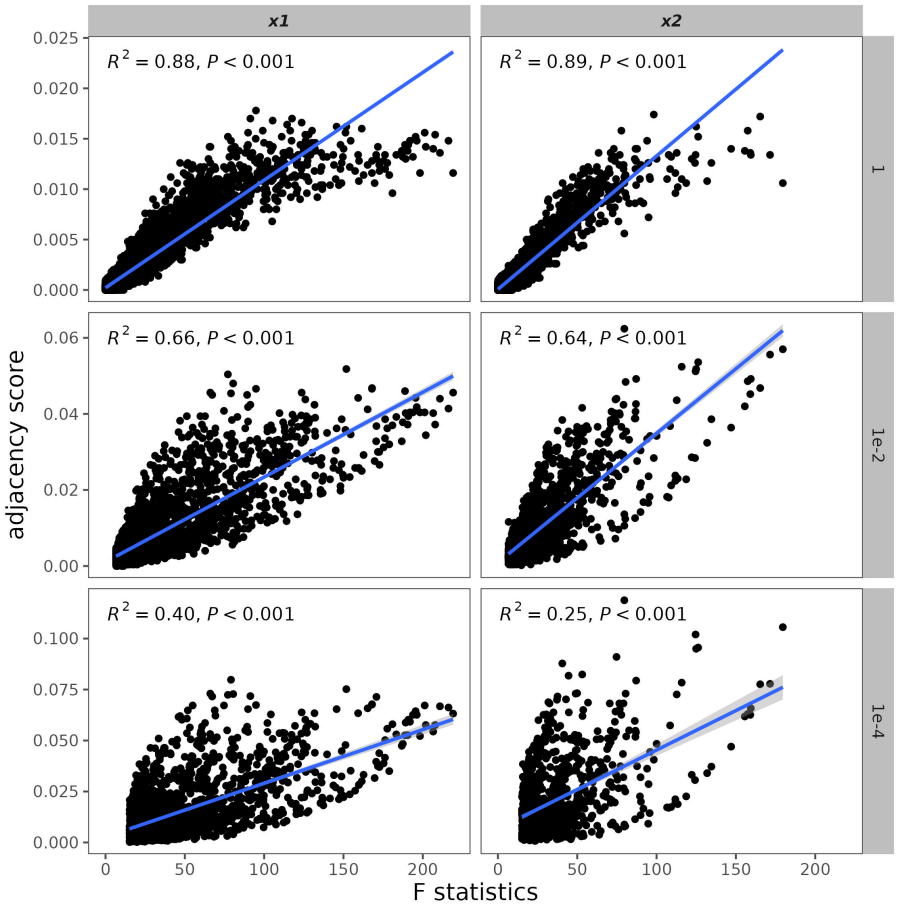

Figure S2: Correlation between F statistics and adjacency scores. The rows represent the P threshold before BN learning, and the columns represent the exposure of interest.

the exposure of interest, and therefore, it is also an assessment of relevance strength.

We explore the correlation between adjacency scores obtained via RGF and F statistics, a widely-used indicator of instrument strength, using the larger simulated dataset (n = 10000, p = 10000). The hyperparameters of RGF are set as n_s = 5000, p_s = 150, r = 1000. Strong positive correlation exists when no primary screening is performed prior to the BN structure learning. With smaller P threshold are used, fewer variants are examined in the RGF, and the correlation strength becomes weaker (Figure S2).

SN3 Performance of BN in the presence of epistasis

We simulate phenotypes from the combination of three polygenetic models including simple multiplicative effects, interactive multiplicative effects, and interactive threshold effects (Table S1) [6], so as to appraise the performance of BN in settling the puzzle of gene interaction and epistasis.

- Simple Multiplicative Model: Each locus individually affects the phenotype with cumulative effects within and between loci. Each additional risk allele increases the effect with a multiplier (θ_1 for allele A and θ_2 for allele B).
- Interactive Multiplicative Model: Both loci interactively affect the phenotype with cumulative effects. Each additional risk allele increases the effect with a multiplier θ only when the risk allele in both loci are present together.
- Interactive Threshold Model: The presence of risk alleles in both loci increases the effect with a multiplier θ without cumulative effects.

Table S1: Polygenetic model

model 1	aa	Aa	AA
bb	α	$\alpha(1+\theta_1)$	$\alpha(1+\theta_1)^2$
Bb	$\alpha(1+\theta_2)$	$\alpha(1+\theta_1)(1+\theta_2)$	$\alpha(1+\theta_1)^2(1+\theta_2)$
BB	$\alpha(1+\theta_2)^2$	$\alpha(1+\theta_1)(1+\theta_2)^2$	$\alpha(1+\theta_1)^2(1+\theta_2)^2$
model 2	aa	Aa	AA
bb	α	α	α
Bb	α	$\alpha(1+\theta)$	$\alpha(1+\theta)^2$
BB	α	$\alpha(1+\theta)^2$	$\alpha(1+\theta)^4$
model 3	aa	Aa	AA
bb	α	α	α
Bb	α	$\alpha(1+\theta)$	$\alpha(1+\theta)$
BB	α	$\alpha(1+\theta)$	$\alpha(1+\theta)$

The complex gene interaction pattern is simulated as combinations of a series of simple patterns (Figure S3). In each simple pattern, phenotype X_1 is determined by loci G_A and G_B through one of the above three polygenetic models, while phenotype X_2 is determined by loci G_A and G_M. Loci G_S is in LD with G_A (S-A) and loci G_T is in reverse LD with G_B (T-b). We set $\pi_A = 0.15$, $\pi_B = 0.20$, $\pi_M = 0.16$, $\pi_S = 0.25$, $\pi_T = 0.3$, $r_AS = 0.7$, $r_BT = -0.6$, $\alpha = 0.2$ for X_1 and $\alpha' = 0.15$ for X_2 in each simple pattern. In simple

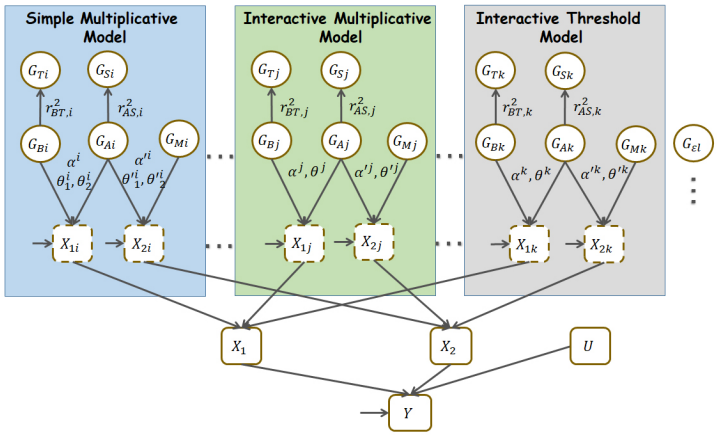

Exposure	Subset	Variants
X_1	$\mathcal{Z}_I$	$G_{Ai}, G_{Bi} (i = 1, \ldots, 20)$
	$\mathcal{Z}_D$	$G_{Si}, G_{Ti} (i = 1, \ldots, 20)$
	$\mathcal{Z}_E$	$G_{Mi} (i = 1, \ldots, 20)$ $G_l (l = 1, \ldots, 900)$
X_2	$\mathcal{Z}_I$	$G_{Ai}, G_{Mi} (i = 1, \ldots, 20)$
	$\mathcal{Z}_D$	$G_{Si} (i = 1, \ldots, 20)$
	$\mathcal{Z}_E$	$G_{Bi}, G_{Ti} (i = 1, \ldots, 20)$ $G_l (l = 1, \ldots, 900)$

Figure S3: The polygenetic model.

multiplicative model, we set $\theta_1 = 0.3$, $\theta_2 = 0.5$ for X_1 and $\theta'_1 = 0.4$, $\theta'_2 = 0.4$ for X_2. In interactive multiplicative model and interactive threshold model, we set $\theta = 0.3$ for X_1 and $\theta' = 0.5$ for X_2. The environmental variance of X_1 is larger to represent traits with lower heritability. The complex pattern is a combination of 60 simple patterns, in which every 20 simple patterns follow a kind of polygenetic model. The ultimate phenotypes X_1 and X_2 is the average of corresponding phenotypes in each simple pattern. We generated other 900 uncorrelated variants. 5000 subjects are sampled in total.

We use the RGF with $n_s = 5000$, $p_s = 150$, $r = 1000$ to select variants belonging to $\mathcal{Z}_D$. The results (Figure S4) reveal that RGF can identify true effect variants with remarkably low false discovery rate (FDR) in the presence of complex gene interaction and epistasis, especially for traits with higher heritability.

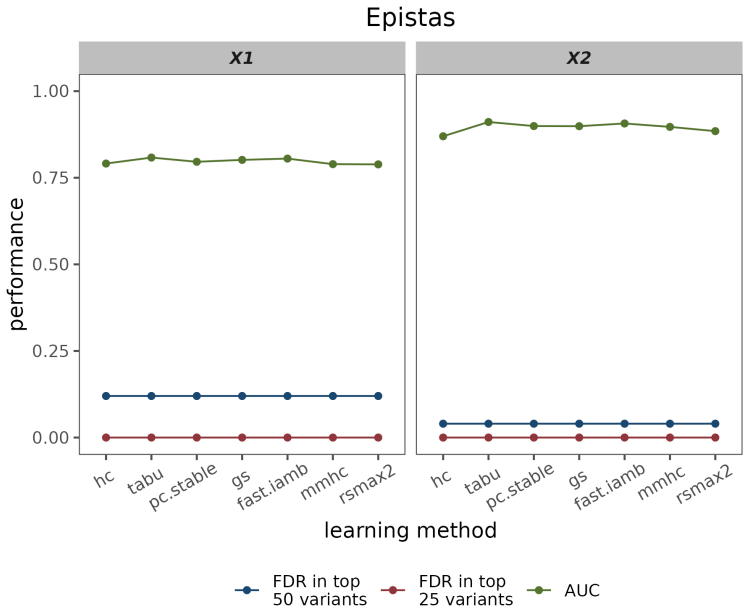

Figure S4: The performance of RGF in the presence of epistasis.

SN4 Sensitivity analysis on IV numbers and iterations

The numbers of iterations and instruments are hyperparameters that need to be specified artificially in advance in BNMR model. For example, one can specify top n^* variants in adjacency scores or variants with adjacency score larger than $\frac{\alpha^* p_s}{p}$ as instruments, where α^* is a given threshold between 0 and 1. Previous researches and experience may benefit the choice but lacks theoretical criteria and explanations. Here we conduct sensitivity analysis using Bayesian MR with different numbers of instruments and iterations in simulations. Instruments are selected according to the ranks of RGF adjacency scores. We want to demonstrate how the changes in hyperparameters affect the properties of estimation (bias, variance, and convergence) as well as time consumption, and examine the stability of BNMR model for different settings.

The sensitivity analysis (Tables S2 & S3, Figures 5 a & b) confirm that robust estimates can be obtained via BNMR. The time consumption increases when the numbers of instruments and iterations increase. Bias increases when there are too many or too few instruments. Good convergence when 5000 iterations have been made according to the Rhat.

Table S2: Sensitivity analysis on different IV number [1]

IV number	time/min	bias	SE	Rhat
10	73.80	2.07	0.064	1.11
20	84.26	2.01	0.031	1.03
40	96.91	2.01	0.027	1.02
60	126.83	2.01	0.025	1.05
100	249.27	2.00	0.025	1.04
150	393.66	2.02	0.024	1.04

[1] The estimation is conducted using simulated data of scenario "50+50" in Table 2. Four chains and 5000 iterations per chain are used under horseshoe prior.

Table S3: Sensitivity analysis on different iterations [1]

IV number	time/min	bias	SE	Rhat
1000	15.01	2.00	0.024	1.22
2000	34.42	2.01	0.029	1.10
5000	64.94	2.00	0.030	1.02
10000	143.69	2.00	0.030	1.01
20000	227.97	2.00	0.029	1.01

[1] 20 instruments are used under horseshoe prior. 60% of them have pleiotropic effects. Four chains are used for sampling.

SN5 Performance of different shrinkage priors

Bayesian estimation with imposed shrinkage priors is conceptually similar to regularization in the traditional model but with some obvious advantages. The penalty parameters can be estimated simultaneously with the model parameters and standard errors of parameters can be obtained directly from posterior distributions. Bayesian models are also more intuitive to establish and interpret, and specific expert knowledge can be included into the model as informative priors. Additionally, Bayesian sampling of posterior distributions though Markov Chain Monte Carlo (MCMC) can avoid the difficulties of traditional regularization methods in solving optimization problems.

We demonstrate the performance of different shrinkage priors in Bayesian MR estimation using RStan [7]. Here we discuss the following commonly used priors [8].

- Bayesian Lasso

$$\begin{aligned} \gamma_j|\lambda &\sim Double-Exp(0,\frac{1}{\lambda}) \\ \lambda &\sim Cauchy^{+}(0,1) \end{aligned} \tag{S.10}$$

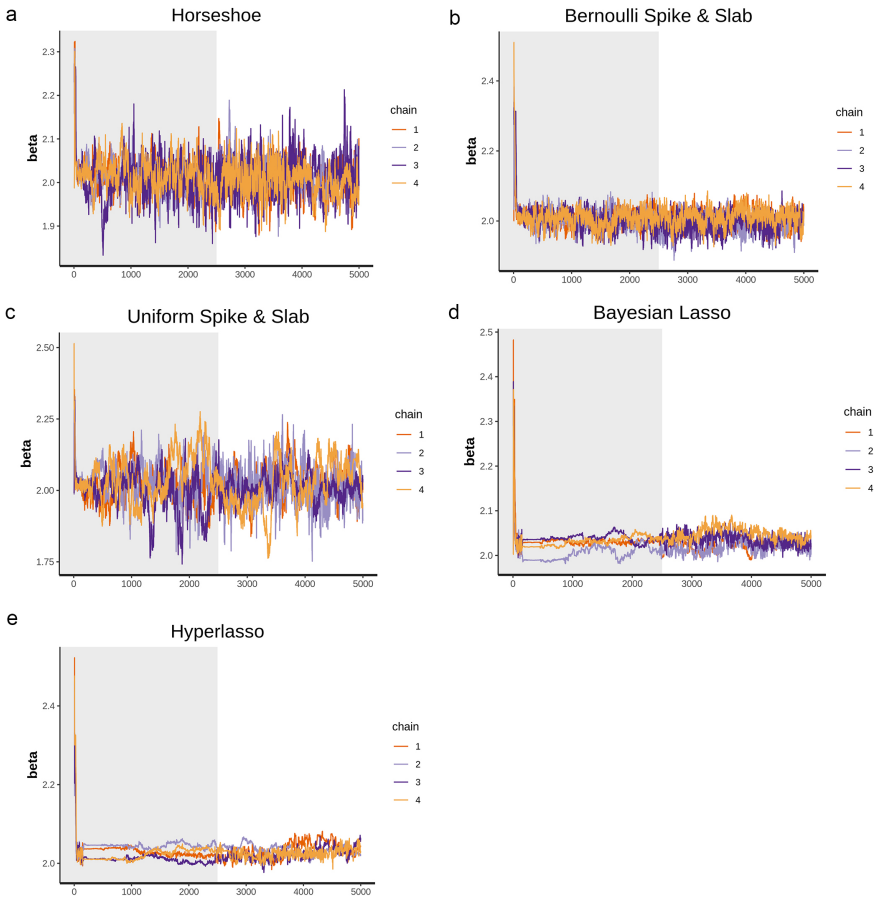

Figure S5: The trace plots of MCMC with different shrinkage priors.

- Hyperlasso

$$\begin{aligned} \gamma_j|\tau_j &\sim Double-Exp(0,\sqrt{2\tau_j}) \\ \tau_j|\lambda &\sim \Gamma(0.5,\frac{1}{\lambda^2}) \\ \lambda &\sim Cauchy^{+}(0,1) \end{aligned} \tag{S.11}$$

- Uniform spike & slab

$$\begin{aligned} \gamma_j|\lambda_j,\tau_j &\sim \lambda_j\mathcal{N}(0,\tau_j) \\ \tau_j &\sim IG(0.5,0.5) \\ \lambda &\sim U(0,1) \end{aligned} \tag{S.12}$$

- Bernoulli spike & slab

$$\begin{aligned} \gamma_j|\lambda_j,\tau_j &\sim \lambda_j\mathcal{N}(0,\tau_j)+(1-\lambda_j)\mathcal{N}(0,0.001) \\ \tau_j &\sim IG(0.5,0.5) \\ \lambda_j|\pi &\sim Bernoulli(\pi) \\ \pi &\sim U(0,1) \end{aligned} \tag{S.13}$$

- Horseshoe

$$\begin{aligned} \gamma_j|\phi_j &\sim N(0,\phi_j) \\ \phi_j|\tau &\sim Cauchy^{+}(0,\tau) \\ \tau &\sim Cauchy^{+}(0,1) \end{aligned} \tag{S.14}$$

Here we use $Cauchy^{+}(\mu,\sigma)$ to represent half-Cauchy distribution with location parameter μ and scale parameter σ, $IG(\alpha,\beta)$ to represent inverse-Gamma distribution with location parameter α and scale parameter β, $Double{-}Exp(\mu,\sigma)$ to represent double-exponential (Laplace) distribution with location parameter μ and scale parameter σ, $\Gamma(\alpha,\beta)$ to represent Gamma distribution with location parameter α and rate parameter β.

Table S4: The performance of different shrinkage priors [1]

prior	time/min	bias	SE	Rhat
horseshoe	57.00	0.007	0.036	1.05
uniform spike & slab	73.96	0.023	0.060	1.11
Bernoulli spike & slab	34.74	0.002	0.025	1.13
lasso	7.90	0.031	0.015	1.36
hyperlasso	45.74	0.034	0.015	1.34

[1] For chains with 5000 iterations per chain and 20 instruments are used.

We use 20 instruments in MR estimations, 60% of which have a pleiotropic effect. There are 5000 iterations in MCMC with 4 chains, and the first half is used as burn-in. The results (Table S4, Figures 5c & S5) show that all these priors can obtain a relatively unbiased estimation. The Bayesian Lasso prior has the fastest sampling speed, while the horseshoe prior is superior in convergence.

SN6 Methods compared in simulations

Here we list and compare the assumptions and methods of different MR estimators in Table S5.

SN7 Empirical coverage

We computed the empirical coverage of the 95% confidence intervals/credible intervals for various methods in each scenario based on 100 repetitions in the

Table S5: Assumptions and methods of compared MR estimators

Method	Data	IV	Accounting for pleiotropy	Assumption	Description
TSLS	individual-level	correlated	No	IV assumptions	The most basic estimator for instrumental variable, requiring that all instruments are valid, and the relationships.
LIML	individual-level	correlated	No	IV assumptions	Applicable to linear structural equation models and more robust in the presence of partial identification issues.
IVW	summary	independent	No	IV assumptions; No measurement error	It combines estimates from individual genetic variants with different weights to produce a pooled estimate. It is more efficient but sensitive to unbalanced pleiotropy.
MR-Egger	summary	independent	Yes	Instrument strength independent of direct effect (InSIDE)	It incorporates an intercept term to estimate the causal effect while allowing for directional pleiotropy under the InSIDE assumption, but less efficient.
Median	summary	independent	Yes	Most (over 50%) weights are valid	It takes the median of the individual variant estimates, weighted by their variances.
Mode	summary	independent	Yes	Zero modal pleiotropy assumption (ZEMPA)	The most (weighted) common causal effect estimate is a consistent estimate of the true causal effect.
JAM-MR	summary	correlated	Yes	Models with homogeneous univariate causal effect are more likely to be valid	JAM-MR performs Bayesian stochastic search through a reversible-jump MCMC algorithm to prioritize genetic variants with strong relevence, and then use of the general Bayesian framework and a heterogeneity-penalizing loss function to get estimate.
CAUSE	summary	i independent	Yes	Variants affect trait M through one of two mechanisms (causal or correlated pleiotropy)	It can handle balanced horizontal pleiotropy.
CIIV	individual-level	correlated	Yes	Plurality rule	It selects the largest group with all CIs overlapping with each other as the set of valid instruments.

simulation. It can be observed that due to the introduction of many correlated loci as background noise in our simulation settings (referring response to question 4), even with very small specified pleiotropic effects, some traditional methods like TSLS, LIML, and IVW have low coverage. MR-Egger and CAUSE exhibit higher coverage, partly because they employ methods to account for pleiotropy effects, and partly because they have lower power, resulting in larger estimation variance and wider confidence intervals. Other methods, including IVW, TSLS, JAM-MR and CIIV, exhibit small estimated standard errors and narrow confidence intervals, which can result in low coverage of the confidence intervals once bias is present, even when the bias is relatively small. The Mode estimator has shown surprising superiority in many cases. NMR does indeed suffer from the impact of uncertainty in the selection stage, and it performs a weaker coverage than CAUSE in scenarios with relatively simple pleiotropic effects. However, this is because CAUSE usually produces a large variance and a very wide confidence interval. In scenarios with more complex pleiotropic structures, methods including BNMR all perform poorly in coverage. Despite this, BNMR still achieved a relatively higher coverage rates in many scenarios, making it a competitive method.

SN8 Instruments used in application

Variants with top 50 adjacency scores are selected as instruments in application. The variants rsID are reported according to Genome Reference Consortium Human Build 37 patch release 13 (GRCh37.p13) (`https://www.ncbi.nlm.nih.gov/assembly/GCF_000001405.25`).

Instruments of RBC

Strict GWAS P threshold (1e-20) in pre-filtering + BNMR:
rs9376090, rs4895440, rs34164109, rs7775698, rs7776054, rs9402685, rs6920211, rs9402686, rs7758845, rs35786788, rs11759553, rs9494142, rs9389269, rs35959442, rs56293029, rs9376091, rs9399137, rs9494145, rs9389268, rs9373124;

Loose GWAS P threshold (5e-8) in pre-filtering with LD clumping (threshold: window = 10000kb, r^2=0.01, MAF=0.01) + BNMR:
rs9399136, rs218265, rs221788, rs9349205, rs10495928, rs9487023, rs550057, rs56397034, rs10224210, rs41294850, rs78744187, rs17476364, rs7137828, rs592423, rs6592965, rs10758656, rs55938136, rs3809627, rs10849020, rs79301522.

Instruments of HGB

Strict GWAS P threshold (1e-20) in pre-filtering + BNMR:
rs72805692, rs17476364, rs79220007, rs1800562, rs16926246, rs79920061, rs16926249, rs113041162, rs55925606, rs73265749, rs144861591, rs1408272, rs80215559, rs115740542, rs10159477, rs10168349, rs198851, rs116009877, rs2032451, rs129128;

Table S6: Empirical coverage of different methods

pleiotropy	scenario	TSLS	LIML	IVW	MR-Egger	Median	Mode	CAUSE	JAM-MR	CIIV_TSLS	CIIV_GMM	BNMR
balanced	50+0	0	0	0.1	0.92	0.58	0.94	1	0.35	0.07	0.07	0.83
balanced	25+25	0.01	0.01	0.09	0.91	0.46	0.94	1	0.16	0	0	0.83
balanced	0+50	0	0	0.07	0.88	0.58	0.95	1	0.3	0.07	0.07	0.8
balanced	100+0	0	0	0.13	0.96	0.54	0.98	1	0.1	0.07	0.07	0.83
balanced	50+50	0.05	0.05	0.2	0.79	0.46	0.97	1	0.1	0.07	0.07	0.7
balanced	0+100	0.06	0.07	0.25	0.84	0.57	0.94	1	0.1	0.27	0.27	0.83
directional	50+0	0	0	0	0.59	0.03	0.57	0.6	0	0	0	0.17
directional	25+25	0	0	0	0.32	0	0.58	0.67	0	0	0	0.5
directional	0+50	0	0	0	0.15	0	0.47	0.6	0	0	0	0.5
directional	100+0	0	0	0	0.2	0	0.13	0.13	0	0	0	0.14
directional	50+50	0	0	0	0.03	0	0.26	0	0	0	0	0.07
directional	0+100	0	0	0	0	0	0.21	0.07	0	0	0	0.14

[1] "the number of independent pleiotropic variants (variants with independent direct effects on both X and Y) + the number of correlated pleiotropic variants (the effects on X and Y are correlated)"".

Table S7: Results of different MR approaches in real data application

exposure	outcome	TSLS			penalized robust MR-Egger			CIIV				BNMR			
		beta	se	P	beta	se	P	beta	se	2.5% CI	97.5% CI	beta	se	2.5% CI	97.5% CI
RBC	DBP	2.239	0.293	0.000	0.444	2.748	0.872	1.426	0.322	0.796	2.057	6.935	0.076	6.472	7.431
RBC	SBP	0.632	0.544	0.246	-0.355	2.759	0.898	-0.359	0.518	-1.374	0.656	8.946	0.067	7.312	10.097
HGB	DBP	1.417	0.131	0.000	1.575	1.309	0.229	1.541	0.187	1.174	1.909	2.226	0.237	1.815	2.608
HGB	SBP	0.446	0.246	0.070	1.872	1.405	0.183	-0.577	0.279	-1.125	-0.030	3.362	0.316	2.738	3.897
HCT	DBP	0.475	0.046	0.000	0.558	0.504	0.268	0.569	0.063	0.446	0.692	0.745	0.256	0.593	0.851
HCT	SBP	0.083	0.087	0.337	0.651	0.529	0.218	-0.219	0.095	-0.404	-0.033	1.093	0.862	0.957	1.214
MCV	DBP	0.031	0.018	0.096	0.154	0.118	0.191	-0.081	0.022	-0.125	-0.038	-0.084	0.065	-0.193	0.038
MCV	SBP	0.025	0.034	0.460	0.076	0.126	0.545	-0.019	0.035	-0.088	0.049	-0.020	0.066	-0.158	0.106

Loose GWAS P threshold (5e-8) in pre-filtering with LD clumping (threshold: window = 10000kb, r^2=0.01, MAF=0.01) + BNMR:

rs17476364, rs144861591, rs1799945, rs10495928, rs7137828, rs635634, rs73158188, rs9402685, rs10901252, rs61739556, rs13107325, rs6665764, rs55893317, rs12819124, rs7778978, rs174533, rs115986297, rs11072567, rs8887, rs123698.

Instruments of HCT

Strict GWAS P threshold (1e-20) in pre-filtering + BNMR:

rs17476364, rs72805692, rs16926246, rs16926249, rs73265749, rs113041162, rs10159477, rs7775698, rs4953318, rs9376090, rs10495928, rs9373124, rs34164109, rs9402685, rs1331309, rs9389269, rs653178, rs9399136, rs9376091, rs9402686;

Loose GWAS P threshold (5e-8) in pre-filtering with LD clumping (threshold: window = 10000kb, r^2=0.01, MAF=0.01) + BNMR:

rs17476364, rs9402685, rs10495928, rs6464165, rs7137828, rs144861591, rs635634, rs1799945, rs221788, rs61739556, rs55893317, rs4282786, rs2732480, rs218265, rs115986297, rs123698, rs13107325, rs4886755, rs2029466, rs55938136.

Instruments of MCV

Strict GWAS P threshold (1e-20) in pre-filtering + BNMR:

rs4895441, rs1800562, rs635243, rs34164109, rs628751, rs55925606, rs66717417, rs112233623, rs9471709, rs9402685, rs589235, rs1799945, rs9373124, rs6920211, rs634869, rs116009877, rs11970772, rs56293029, rs592423, rs1408272;

Loose GWAS P threshold (5e-8) in pre-filtering with LD clumping (threshold: window = 10000kb, r^2=0.01, MAF=0.01) + BNMR:

rs9399136, rs9471708, rs144861591, rs592423, rs198851, rs218265, rs9487023, rs7853365, rs6014993, rs9381093, rs9866958, rs2238368, rs7385804, rs6592965, rs9816784, rs8887, rs56397034, rs41294850, rs4890633, rs62160676.

Instruments of leukocyte count

BNMR:

rs60134943, rs12600856, rs59269632, rs12940405, rs8075668, rs3184504, rs8069202, rs7222039, rs3936197, rs11725704, rs8078692, rs2270401, rs9914973, rs445, rs62066853, rs9378212, rs1548306, rs11574938, rs4760, rs3902025

MR-Egger and weighted Median:

rs12266014, rs10995477, rs10786327, rs3184504, rs2038700, rs11574938, rs247826, rs12600856, rs2665405, rs78663649, rs4760, rs7255933, rs3917932, rs34293785, rs2476601, rs2208568, rs1260326, rs6740847, rs16850073, rs11725704, rs10075801, rs2594836, rs2524079, rs9270636, rs7776054, rs2158799, rs56388170, rs445, rs7846314, , rs59697075

Instruments of lymphocyte count

BNMR:

rs3184504, rs11066283, rs77600511, rs875622, rs1265564, rs113627332, rs4766897, rs2034892, rs9264904, rs2442728, rs8109817, rs55908509, rs1386622, rs142000971, rs13063578, rs73516986, rs1265565, rs12459007, rs2286599, rs11574938

MR-Egger and weighted Median:

rs6589939, rs10466905, rs3184504, rs3812849, rs3540, rs11574938, rs247826, rs36084354, rs5498, rs10875338, rs2476601, rs4618126, rs5754100, rs714027, rs72781680, rs149290349 rs13431440, rs59395276, rs1822534, rs13063578, rs13092376 rs1386622, rs12504282, rs62355272, rs2853950, rs9494142, rs3735485, rs2919917, rs6475611

Instruments of monocyte count

BNMR:

rs12346772, rs1375493, rs10980797, rs60698178, rs155123, rs155144, rs62525615, rs9695374, rs391855, rs2270502, rs3829729, rs2713575, rs62273237, rs148016591, rs11117426, rs10817154, rs10094039, rs10980823, rs34347479, rs824016

MR-Egger and weighted Median:

rs12266014, rs11189122, rs1945392, rs1800973, rs653178, rs1892548, rs12874404, rs2239630, rs2038700, rs8022179, rs72726034, rs7180079, rs12916091, rs8026803, rs391855, rs6540234, rs8081108, rs7212590, rs1037171, rs344812, rs10418046, rs78539283, rs4970966, rs9970896, rs12480732, rs6125961, rs2869981, rs7288670, rs138918, rs13022141, rs1375493, rs6757927, rs2228467, rs2213290, rs6782228, rs10004764, rs13138355, rs17656204, rs2844578, rs7776054, rs6796, rs4385425, rs445, rs13271228, rs62525615, rs6475611, rs9410380, rs10980797 rs314462,

Instruments of depression

BNMR:

rs3823612, rs11660187, rs10119773, rs4799959, rs769685, rs1427027, rs11661202, rs1427028, rs2056477, rs4632195, rs1431188, rs769688, rs3793577, rs7231178, rs62097987, rs62097980, rs7230446, rs17501820, rs10502971, rs62097899

MR-Egger and weighted Median:

rs11214469, rs1427027, rs8099160, rs589092, rs769688, rs3823612, rs10119773, rs10123378

SN9 Comparison with conventional methods in case studies

We conduct the MR analysis using existing MR procedures. In Table S5, we report estimates from our BNMR method and other three existing approaches (TSLS, penalized robust MR-Egger, and CIIV). The conpared methods use lead SNPs after LD clumping by R package ieugwasr as instruments. TSLS is implemented with R package AER, penalized robust MR-Egger estimator is

implemented with R package MendelianRandomization [9], and CIIV is implemented with R package CIIV. We can find that estimates vary significantly when using different IVs and MR approaches.

The results indicate that appropriate instruments and estimation methods are vital in MR analysis. The results of MR should be taken with caution, and need more triangulating evidence from other non-MR designs [10].

SN10 Gene mapping and functional annotation for depression

Figure S shows the results of canonical pathway enrichment of depression-related SNPs mapped genes. We can find depression-related genes indicates enrichment in many cytokine and immune response pathways, including reactomes related to signaling of interleukin 9, Wnt, biocarta, and butyrophilin family.

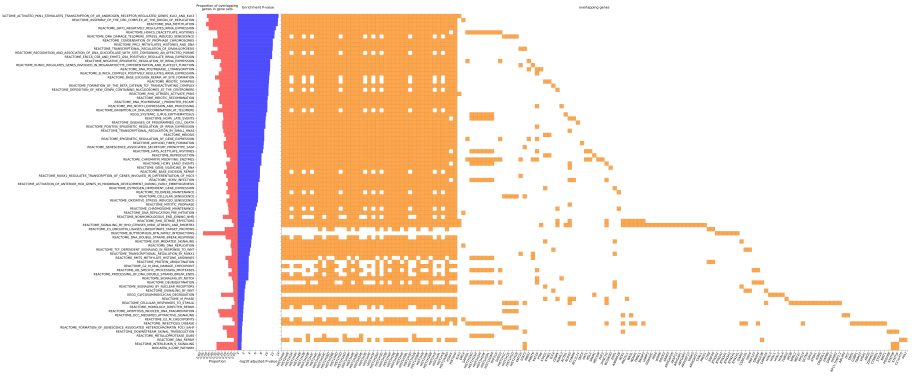

Figure S6: Canonical pathway enrichment of depression-related SNPs mapped genes.

SN11 Another example with limited samples

We provided another example of BNMR with fewer samples. Lymphocyte count is reported to be associated with psychiatric disorders like schizophrenia (SCZ) and post-traumatic stress disorder (PTSD). Using UK Biobank, 411 subjects with SCZ and 253 subjects with PTSD are included, and we sample 1000 subjects without psychiatric disorders to balance the sample. All participants are of Caucasian ancestry. Reciprocal MR analysis is conducted to avoid reverse causation. Results from both BNMR and MR-Egger indicate that lymphocyte count has a positive effect on SCZ but have no significant effect on PTSD. Using top 1500 SNPs selected by RGF, FUMA maps 36 SCZ-related protein-coding genes. MAGMA tissue expression analysis reveals an enrichment of SCZ-related

genes in the thyroid, the organ secreting hormones as essential immune modulators. The secretion is regulated by dopamine, an essential neuro-immune-transmitter that has been a focus of SCZ aetiology research for decades because a deficit in dopamine release is reported in SCZ patients [11]. SCZ is reported to be associated with immune system dysfunction, manifesting in abnormal blood immune parameters [12]. Meanwhile, lymphocytes participate in the synthesis of dopamine and its metabolites, and abnormalities in dopamine receptor expression in lymphocytes are observed in SCZ patients [13]. Previous MR research identified the protective effects of long-chain ω-3 and ω-6 fatty acids on SCZ [14]. Meanwhile, substantial evidence from both population research and cellular experiments demonstrates that decreases in fatty acids cause lymphocyte expansion [15]. A possible causal pathway may be plasma fatty acids → lymphocyte → dopamine → SCZ. However, this assumption should be taken with cautious, since the sample size is limited in one-sample study, and more evidence is needed to support further conclusions.

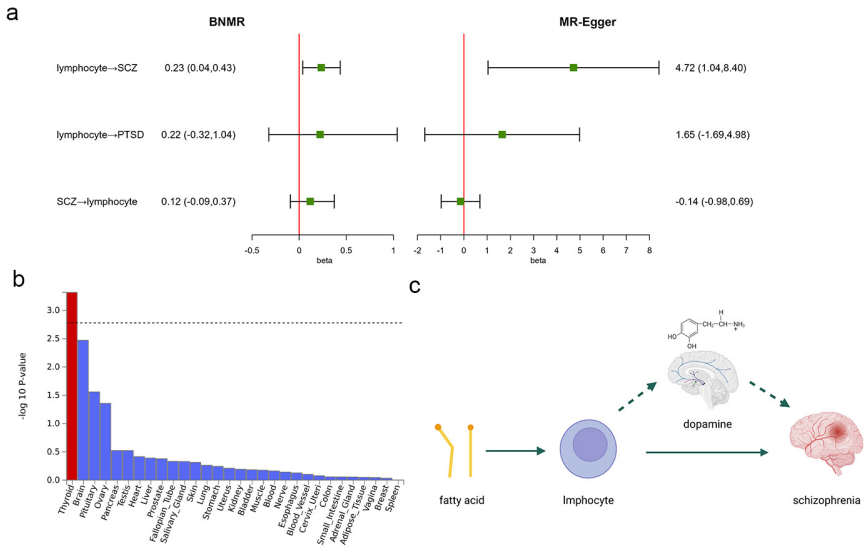

Figure S7: The relationships between lymphocyte count and psychiatric disorders. **a**. Forest plot of the causal estimations of BNMR and MR-Egger. The unit of lymphocyte count is billion cells per liter. For BNMR, we select 20 instruments for each exposure via RGF (n_s = 4000, p_s = 150, r = 5000), shown in Supplementary Note SN6, and sample 4 chains with 5000 iterations per chain in MCMC. For MR-Egger, GWAS lead variants after LD clumping are selected as instruments. **b**. MAGMA tissue expression analysis for mapped SCZ-related genes in GTEx v8 30 general tissue types. **c**. A potential causal pathway of SCZ: fatty acids regulate the lymphocyte counts, and lymphocytes contribute to the development of SCZ by participating in dopamine metabolism.

References

[1] Richard Howey, So-Youn Shin, Caroline Relton, George Davey Smith, and Heather J Cordell. Bayesian network analysis incorporating genetic anchors complements conventional Mendelian randomization approaches for exploratory analysis of causal relationships in complex data. *PLoS Genetics*, 16(3):e1008198, 2020.

[2] Ana Rita Nogueira, Andrea Pugnana, Salvatore Ruggieri, Dino Pedreschi, and João Gama. Methods and tools for causal discovery and causal inference. *Wiley Interdisciplinary Reviews: Data Mining and Knowledge Discovery*, 12(2):e1449, 2022.

[3] Marco Scutari. Learning Bayesian networks with the bnlearn R package. *Journal of Statistical Software*, 35(3):1–22, 2010.

[4] Jean-Baptiste Pingault, Paul F O'reilly, Tabea Schoeler, George B Ploubidis, Frühling Rijsdijk, and Frank Dudbridge. Using genetic data to strengthen causal inference in observational research. *Nature Reviews Genetics*, 19(9):566–580, 2018.

[5] Carlo Berzuini, Hui Guo, Stephen Burgess, and Luisa Bernardinelli. A Bayesian approach to Mendelian randomization with multiple pleiotropic variants. *Biostatistics*, 21(1):86–101, 2020.

[6] Jonathan Marchini, Peter Donnelly, and Lon R Cardon. Genome-wide strategies for detecting multiple loci that influence complex diseases. *Nature Genetics*, 37(4):413–417, 2005.

[7] Bob Carpenter, Andrew Gelman, Matthew D Hoffman, Daniel Lee, Ben Goodrich, Michael Betancourt, Marcus Brubaker, Jiqiang Guo, Peter Li, and Allen Riddell. Stan: A probabilistic programming language. *Journal of Statistical Software*, 76(1), 2017.

[8] Sara Van Erp, Daniel L Oberski, and Joris Mulder. Shrinkage priors for Bayesian penalized regression. *Journal of Mathematical Psychology*, 89:31–50, 2019.

[9] Olena O Yavorska and Stephen Burgess. Mendelianrandomization: an R package for performing Mendelian randomization analyses using summarized data. *International Journal of Epidemiology*, 46(6):1734–1739, 2017.

[10] Debbie A Lawlor, Kate Tilling, and George Davey Smith. Triangulation in aetiological epidemiology. *International Journal of Epidemiology*, 45(6):1866–1886, 2016.

[11] Jodi J Weinstein, Muhammad O Chohan, Mark Slifstein, Lawrence S Kegeles, Holly Moore, and Anissa Abi-Dargham. Pathway-specific dopamine abnormalities in schizophrenia. *Biological Psychiatry*, 81(1):31–42, 2017.

[12] Brian J Miller, Bintou Gassama, Dale Sebastian, Peter Buckley, and Andrew Mellor. Meta-analysis of lymphocytes in schizophrenia: clinical status and antipsychotic effects. *Biological Psychiatry*, 73(10):993–999, 2013.

[13] MA Penedo, T Rivera-Baltanás, D Pérez-Rodríguez, J Allen, A Borrajo, D Alonso-Crespo, C Fernández-Pereira, M Nieto-Araujo, S Ramos-García, C Barreiro-Villar, et al. The role of dopamine receptors in lymphocytes and their changes in schizophrenia. *Brain, Behavior, & Immunity-Health*, 12:100199, 2021.

[14] Hannah J Jones, Maria Carolina Borges, Rebecca Carnegie, David Mongan, Peter J Rogers, Sarah J Lewis, Andrew D Thompson, and Stanley Zammit. Associations between plasma fatty acid concentrations and schizophrenia: a two-sample Mendelian randomisation study. *The Lancet Psychiatry*, 8(12):1062–1070, 2021.

[15] Darshan S Kelley. Modulation of human immune and inflammatory responses by dietary fatty acids. *Nutrition*, 17(7-8):669–673, 2001.